

THESIS FOR THE DEGREE OF LICENTIATE OF ASTRONOMY

From Photons to Worlds

ISKRA GEORGIEVA



CHALMERS
UNIVERSITY OF TECHNOLOGY

Division of Astronomy and Plasmaphysics
Department of Space, Earth and Environment
Chalmers University of Technology
Gothenburg, Sweden, 2021

From Photons to Worlds

ISKRA GEORGIEVA

Copyright © 2021 ISKRA GEORGIEVA
All rights reserved.

Technical Report No. 2021-0064
ISSN 3.1415-9265
This thesis has been prepared using L^AT_EX.

Division of Astronomy and Plasma physics
Department of Space, Earth and Environment
Chalmers University of Technology
SE-412 96 Gothenburg, Sweden
Phone: +46 (0)31 772 1000
www.chalmers.se

Printed by Chalmers Reproservice
Gothenburg, Sweden, June 2021

Abstract

Since the first unambiguous detection of a planet around a Sun-like, the interest in the new and exciting field of exoplanets has grown immensely. New and exciting developments are seen at a pace unparalleled for most subfields of astronomy and astrophysics.

In this thesis, I describe the two most successful techniques for exoplanet detection and characterisation – transits and radial velocities – and the challenges commonly encountered in extracting the planets from the data.

Transit photometry allows us to measure the planet radius, while radial velocity measurements give us the planet's minimum mass. These methods' true strength, however, manifests in their combination as it allows us to estimate the true mass, which together with the radius gives us an estimate of a planet's bulk density. This is a powerful quantity, which allows us to speculate about the structure and composition of a planet's interior and atmosphere.

I describe the process of detecting a planet in a stellar light curve, and how transits and radial velocities are modelled together in order to determine the planet parameters. I demonstrate how the ideal theoretical approach can be used to study a system in practice. However, the current challenges in exoplanet characterisation surpass the ideal case, leading us to explore more complex models. Finally, I show how by extending the ideal planet approach with non-parametric models, we can detect planets in complicated datasets, as demonstrated by the case of the TOI-1260 multi-planet system.

Keywords: Exoplanet, planetary systems, transits, radial velocities.

List of Publications

This thesis is based on the following publications:

[A] **I. Y. Georgieva**, C. M. Persson, O. Barragán, G. Nowak, M. Fridlund, D. Locci, E. Pale, R. Luque, I. Carleo, D. Gandolfi, S. R. Kane, J. Korth, K. G. Stassun, J. Livingston, E. C. Matthews, K. A. Collins, S. B. Howell, L. M. Serrano, S. Albrecht, A. Bieryla, C. E. Brasseur, D. Ciardi, W. D. Cochran, K. D. Colon, I. J. M. Crossfield, Sz. Csizmadia, H. J. Deeg, M. Esposito, E. Furlan, T. Gan, E. Goffo, E. Gonzales, S. Grziwa, E. W. Guenther, P. Guerra, T. Hirano, J. M. Jenkins, E. L. N. Jensen, P. Kabáth, E. Knudstrup, K. W. F. Lam, D. W. Latham, A. M. Levine, R. A. Matson, S. McDermott, H. L. M. Osborne, M. Paegert, S. N. Quinn, S. Redfield, G. R. Ricker, J. E. Schlieder, N. J. Scott, S. Seager, A. M. S. Smith, P. Tenenbaum, J. D. Twicken, R. Vanderspek, V. Van Eylen, J. N. Winn, “Hot planets around cool stars – two short-period mini-Neptunes transiting the late K-dwarf TOI-1260”. Accepted for publication in *Monthly Notices of the Royal Astronomical Society*.

Other publications by the author, not included in this thesis, are:

[B] R. Luque, ..., **I. Georgieva**, et al, “A planetary system with two transiting mini-Neptunes near the radius valley transition around the bright M dwarf TOI-776”. *A&A*, 2021, 645, 41.

[C] M. Fridlund, ..., **I. Georgieva**, et al, “The TOI-763 system: sub-Neptunes orbiting a Sun-like star”. *MNRAS*, 2020, 498, 4503.

[D] I. Carleo, ..., **I. Georgieva**, et al, “The Multiplanet System TOI-421 – a warm Neptune and a super puffy mini-Neptune transiting a G8 V star in a visual binary”. *AJ*, 2020, 160, 114 .

[E] G. Nowak, ..., **I. Georgieva**, et al, “K2-280 b - a low density warm sub-Saturn around a mildly evolved star”. *MNRAS*, 2020, 497, 4423.

[F] P. Bluhm, ..., **I. Georgieva**, et al, “Precise mass and radius of a transiting super-Earth planet orbiting the M dwarf TOI-1235: a planet in the radius gap?”. *A&A*, 2020, 639, 132.

- [G] J. Šubjak, ..., **I. Georgieva**, et al, “TOI-503: The First Known Brown-dwarf Am-star Binary from the TESS Mission”. *AJ*, 2020, 159, 151.
- [H] D. Hidalgo, ..., **I. Georgieva**, et al, “Three planets transiting the evolved star EPIC 249893012: a hot $8.8\text{-}M_{\oplus}$ super-Earth and two warm 14.7 and $10.2\text{-}M_{\oplus}$ sub-Neptunes”. *A&A*, 2020, 636, 89.
- [I] M.R. Díaz, ..., **I. Georgieva**, et al, “TOI-132 b: A short-period planet in the Neptune desert transiting a $V = 11.3$ G-type star”. *MNRAS*, 2020, 493, 973.
- [J] L.D. Nielsen, ..., **I. Georgieva**, et al, “Mass determinations of the three mini-Neptunes transiting TOI-125”. *MNRAS*, 2020, 492, 5399.
- [K] C.X. Huang, ..., **I. Georgieva**, et al, “TESS Spots a Hot Jupiter with an Inner Transiting Neptune”. *ApJL*, 2020, 892, 7.
- [L] K.W.F. Lam, ..., **I. Georgieva**, et al, “It Takes Two Planets in Resonance to Tango around K2-146”. *ApJ*, 2020, 159, 120.
- [M] C.M. Persson, ..., **I. Georgieva**, et al, “Greening of the brown-dwarf desert. EPIC 212036875b: a $51\text{ }M_J$ object in a 5-day orbit around an F7 V star”. *A&A*, 2019, 628, 64.

Acknowledgments

I would firstly like to thank my main supervisor Carina Persson and my co-supervisor Malcolm Fridlund for perhaps taking a leap of faith in hiring me instead of someone with a continuous background in the astrophysical sciences. I hope I am living up to your expectations. I am also grateful for your support in the sub-smooth experience that writing my first paper has been. I have undoubtedly learned a lot.

I am especially thankful to OB for being as good a collaborator as he is a friend. I look forward to more adventures, both professional and casual.

Finally, a massive thank you! to all my peeps here at AoP for helping to keep me sane during these difficult times – I hope to have contributed to any remaining sanity you have as well.

Acronyms

ARIEL:	Atmospheric remote-sensing infrared exoplanet large survey
AU:	Astronomical unit
CHEOPS:	Characterising exoplanet satellite
CoRoT:	Convection, rotation and planetary transits
CCF:	Cross-correlation function
EB:	Eclipsing binary
ESPRESSO:	Echelle spectrograph for rocky exoplanets and stable spectroscopic observations
EXPRES:	Extreme precision spectrograph
FOV:	Field of view
GP:	Gaussian process
HabEx:	Habitable exoplanet observatory
HARPS:	High accuracy radial velocity planet searcher
JWST:	James Webb space telescope
KST:	Kepler space telescope
LUVOIR:	Large UV/Optical/Infrared surveyor
MCMC:	Markov chain Monte Carlo
PLATO:	Planetary transits and oscillations
RV:	Radial velocity
TESS:	Transiting exoplanet survey satellite

Definitions

This section contains a non-exhaustive list of notation and constants in SI units commonly used throughout this work. The values are as per Prša et al. (2016).

- M_{\star} – stellar mass
- R_{\star} – stellar radius
- M_{p} – planet mass
- R_{p} – planet radius
- M_{\odot} – Solar mass, 1.988×10^{30} kg
- R_{\odot} – Solar radius, 6.957×10^8 m
- M_{\oplus} – Earth mass – 5.971×10^{24} kg
- R_{\oplus} – Earth radius – 6.3781×10^6 m
- M_J – Jupiter mass – 1.898×10^{27} kg
- R_J – Jupiter radius – 7.1492×10^7 m
- AU – Astronomical unit – 1.496×10^{11} m
- pc – parsec – 3.086×10^{16} km

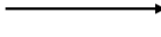
Spectral class	Mass, M_{\odot}	Radius, R_{\odot}	Effective temperature, K	Fraction from all main-sequence stars, %
Early	≥ 18	≥ 7.2	$\geq 31,500$	~ 0.00003
	2.3 - 18	2.2 - 7.2	10,000 - 31,500	0.13
	1.7 - 2.3	1.75 - 2.2	7,300 - 10,000	0.6
	1.07 - 1.7	1.13 - 1.75	6,000 - 7,300	3
	0.9 - 1.07	0.83 - 1.13	5,300 - 6,000	7.5
	0.58 - 0.9	0.6 - 0.83	3,900 - 5,300	12
	0.08 - 0.58	≤ 0.6	2,300 - 3,900	75
Late				

Table 0.1: Basic stellar spectral classification. The values and ranges are as per Pecaut & Mamajek (2013) and are approximate.

Contents

Abstract	i
List of Papers	ii
Acknowledgements	iv
Acronyms	v
Definitions	vi
1 Introduction	1
1.1 What is an exoplanet?	2
1.2 Exoplanet detection	5
The transit method	5
The radial velocity method	11
1.3 Exoplanet demographics	14
2 A closer look at the theory behind transits and radial velocities	17
2.1 Orbital elements	17
2.2 Transit method	18
Transit observables	18
Other physical quantities	21

Challenges and caveats	23
2.3 Radial velocity method	25
Combining the two methods	26
Challenges	27
3 From photons to worlds	31
3.1 Finding transits in light curve data	31
3.2 Joint modelling of transits and RVs	34
The harsh reality	37
4 Paper summary	39
4.1 Paper A	39
5 Outlook	43
5.1 Concluding remarks	43
5.2 Reflection and Future work	44
Bibliography	47
A TOI-1260	A1

CHAPTER 1

Introduction

For thousands of years the solar system planets were the only planets whose existence humanity was aware of. Iconic images of the planets and their moons obtained by famous Solar system missions, like the Pioneer, Mariner, Viking, Voyager and Cassini probes, have inspired generations of young minds. But our knowledge of planetary physics was completely based on the bodies gravitationally bound to our Sun.

This began to change only a few decades ago when the family of known planets extended beyond the Solar system, when the first planets around a pulsar¹ were unambiguously confirmed in 1992 (Wolszczan & Frail 1992), followed by the discovery of the first planet around a Sun-like star in 1995 (Mayor & Queloz 1995). The latter was awarded the Nobel prize in physics in 2019.

Since these first discoveries, the field of exoplanetology has exploded.

But why did it take so long?

While a complete answer to this question is multi-faceted, possibly the simplest one is that exoplanets are billions of times fainter than their host stars.

¹A compact stellar remnant, which emits electromagnetic pulses of radiation, mostly in radio.

Adding the fact that they are small and far away, to this day, they are extremely difficult to find by direct imaging, which is the first technique for astronomical observations that became available². We had to wait for the invention of other sophisticated indirect methods and even longer, for the technological leaps needed to realise them. What is more, we can now not only detect the planets, but also begin to characterise them by finding out information about them, the systems they inhabit, their environment and history, by observation and modelling. These advances will eventually enable us to answer questions regarding the place of the Solar system, and specifically the Earth, in the tapestry of the current exoplanet census.

This thesis focuses on the two currently most common and successful exoplanet discovery techniques, what information they provide that allows us to characterise the planets, and the modelling strategies we adopt that enable us to accomplish this.

But first things first...

1.1 What is an exoplanet?

It may come as a surprise, but coming up with a general but strict definition for a planet is not straight-forward.

Definitions

Starting from the official definition of a planet in the Solar system adopted by the International Astronomical Union (IAU) in 2006³, in order for a body to be classified as a planet, it must fulfil three requirements:

1. the body orbits the Sun.
2. it has sufficient mass for its self-gravity to overcome rigid body forces so that it assumes hydrostatic equilibrium (nearly round) shape.
3. it has cleared the neighbourhood around its orbit.

²Galileo Galilei was the first observational astronomer who used a telescope to observe the heavens in the early 17th century.

³The specific resolutions can be consulted at: https://www.iau.org/static/resolutions/Resolution_GA26-5-6.pdf

In the context of exoplanets, however, this definition needs to be extended and generalised since it addresses only the lower limit of a planet’s mass. This is not practically useful since current observations cannot yet detect dwarf planets⁴ around distant stars, and thus a distinction between exoplanets and smaller bodies is not yet as pertinent as the upper planetary mass bound. The IAU recommendation from 2003 is that the limit between sub-stellar bodies (brown dwarfs) and regular planets should be taken to be the calculated mass limit required for the onset of deuterium burning, i.e. $\sim 13 M_J$. This has, however, been challenged by a number of authors (e.g. Soter 2006; Chabrier et al. 2014; Hatzes & Rauer 2015; Persson et al. 2019), with a general consensus that an upper planetary mass limit should be significantly higher. In this work, I will use $\sim 75 M_J$ as an upper limit for bodies of planetary nature, which roughly corresponds to the onset of hydrogen burning.

Planet categories

The over 4300 exoplanets discovered to date (including confirmed planets with both mass and radius, and statistically validated ones) show us that planets can be categorised by radius (Borucki et al. 2011), and mass (Charbonneau et al. 2009; Stevens & Gaudi 2013) in the following way:

- Terrestrial, Earth-like – $R < 1.25 R_\oplus$, $M < 2 M_\oplus$
- Super-Earths – $R \sim 1.25 - 2 R_\oplus$, $M \sim 2 - 10 M_\oplus$
- Neptunes – $R \sim 2 - 6 R_\oplus$, $M \sim 10 - 100 M_\oplus$
- Giant planets – $R \sim 6 - 15 R_\oplus$, $M \sim 0.3 - 75 M_J$

These categories are broad and are by no means strict definitions as other physically motivated bounds exist. Moreover, the transition from one planet type to another is smooth and it is thus often difficult to distinguish between them. One such important blurred region is the one between the upper end of the super-Earth and the lower end of the Neptunes, as will be described below. But first, let us have a look at some basic characteristics of the different planet classes.

⁴IAU definition: a celestial body that orbits the Sun, has enough mass to assume a nearly round shape, has not cleared the neighborhood around its orbit, and is not a moon.

Earth-like planets are considered to have an Earth-like composition, i.e. silicate rock and metals, similar to the terrestrial planets in the Solar system (Mercury, Venus, Earth and Mars). Apart from a metallic core and a silicate mantle, terrestrial planets may also feature secondary, possibly outgassed, atmospheres.

Super-Earths have something in common with the lower end of the Neptune-size planets, the so-called **mini-Neptunes** ($2-3 R_{\oplus}$). Apart from not having an analog in our Solar system, these two groups share the inconvenience that their composition cannot be uniquely constrained solely by knowing their bulk densities (i.e. mass and radius). They are inferred to range from abundant in H-He on the low density end, through H₂O-rich, to being terrestrial (solid surface) with or without an atmosphere, at the high density end.

Neptunian planets, as the name suggests, are considered to be similar to Uranus and Neptune, containing significant mass fractions of ices, rock, as well as H and He.

Finally, **giant planets** – Jupiters, super-Jupiters and brown dwarfs – are loosely constrained to have $> 50\%$ H-He by mass with atmospheres accreted from the original nebula (i.e. primary atmospheres).

Planet nomenclature

The names of exoplanets have two parts – 1) a word or abbreviation, sometimes followed by numbers, and 2) a lower-case letter. The first part is the name of the star – either its catalogue name or the name of the instrument or facility that discovered it. Stars can have multiple designations as they may exist in different catalogues, but famous catalogue names (e.g. GJ or HD) take precedence over instrument names, wherever possible.

The second part of the name, the letter, tells of the order in which the planet was discovered. The first planet that is discovered in a system is given the letter b, followed by letters c, d, and so on, for every subsequent planet found in the system. Often the inner-most planet is found first, and it is given the letter b. If multiple planets are discovered at the same time, they are given letters b, c, d, and so on, in order of their distance from the star. This, however, is not always the case.

The names of planets orbiting binary (or multiple) stars can be somewhat confusing. For example, a planet orbiting the binary Kepler-16AB is named Kepler-16(AB)b.

1.2 Exoplanet detection

The nearest exoplanet to Earth orbiting the closest star to the Sun is Proxima Centauri b. One would think that it being located at roughly 1.3 pc away from us would allow us to use a direct technique, like imaging, to study it. Unfortunately, since it is so close to its star that it takes 11.2 days to complete an orbit around it, it is drowning in the star's glare. And this is true for planets several AU⁵ away from their stars. In fact, if we base our expectations of exoplanets on the Solar system planets, we would find many surprises. One of them is that a large fraction of the exoplanets found to date have similar, and even shorter orbital periods to Proxima Centauri b. Thus, at least for now, we rely on indirect methods to detect and study exoplanets.

Below I outline the two most well-known such methods, which have yielded about 95%⁶ of the confirmed exoplanets known to date, and represent the foundation of this work. These are the **transit** and the **radial velocity** (RV) methods. Other successful detection methods exist, the most note-worthy of which, in decreasing order of exoplanet yield, are microlensing (Bond et al. 2004), direct imaging (Boccaletti 2011) and transit timing variations (TTVs, Ballard et al. 2011). These will not be described in detail in this work and the interested reader is referred to the references in the text.

Neither of these is a novel method – both were discussed by (Struve 1952) – but it was not until the end of the last century when they were successfully utilised for exoplanet detection. The field of exoplanets has exploded since then, thanks to concentrated effort in improving the instrumentation and growing interest since the early discoveries.

The transit method

The fundamental idea of a transit is simple and most of us have likely seen a transit at least once. In fact, a transit is a special case of an eclipse, such that a smaller body obscures the light from a larger one when it passes in front of it. If the inclination of a planet's orbit around its host star is close to 90° in the plane of the sky (i.e. edge-on orbit has $i = 90^\circ$), then the presence of this planet can be inferred by detecting the periodic dips of stellar flux

⁵The Astronomical Unit is the average distance from the Earth to the Sun.

⁶This value, together with abundant information about exoplanets can be found at: <https://exoplanetarchive.ipac.caltech.edu/>

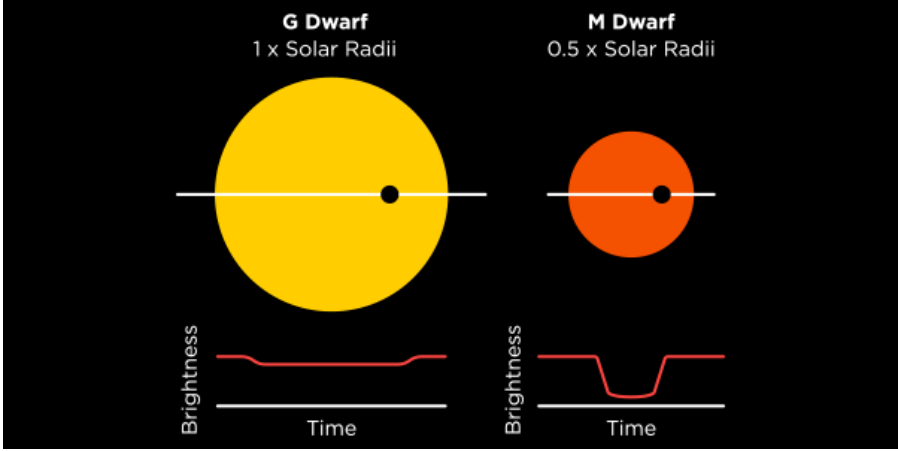


Figure 1.1: Illustration of a planetary transit. Comparison between the same planet transiting a Sun-like star (left) and a smaller, less bright star (right). This difference in transit depth demonstrates why it is easier to detect smaller planets around less massive stars. Image credit: The Center for Astrophysics | Harvard & Smithsonian.

caused by the partial occultation of the stellar disc (see Fig. 1.1). Intuitively, the missing flux, i.e. the transit depth, can thus be related to the size of the planet blocking the star. If we do not know the size of the star, we will at least know the size ratio of the planet and the star, R_p/R_* . Thankfully, nowadays we usually have relatively precise estimates of stellar radii through spectroscopy, combined with parallax and photometry. This, combined with the periodicity of the dips, gives us the first fundamental parameters: the planet’s radius, orbital period and distance from the star.

Unfortunately, a transit can only be seen by an observer if the orbital geometry of the system is favourable. Given interstellar distances, a transit would be visible if the portion of the celestial sphere swept out by the planet’s shadow is in the line of sight of an observer on Earth. Assuming the orbital inclination of planets is random and that the planet radius is small compared to the stellar radius such that $R_p \ll R_*$, the probability of a transit is $\approx 0.0046 (R_*/R_\odot) (1\text{AU}/a)$, where R_* is the radius of the host star, R_\odot – the radius of the Sun, and a – the semi-major axis of the planet’s orbit. So if a planet orbits a Sun-like star at a distance of 1 AU, the probability of a transit

is just 0.46%, while at the distance of Jupiter (5.2 AU), this probability drops to 0.09%. More generally, this expression shows that the planets we are most likely to detect using the transit method, as shown in Fig. 1.2, are hot planets in close orbits to their stars. Furthermore, a transiting Jupiter around a star the size of the Sun (a G-type star) would cause a dip of about 1%, while an Earth-size planet would only result in about 0.01% loss of total flux. The square of the stellar radius is inversely proportional to the transit depth (see Chapter 2), so smaller, less luminous stars, such as M and K stars (Table 0.1), would cause a much larger reduction in flux, as illustrated in Fig. 1.1 (Collier Cameron 2016).

Transit surveys

Consequently, to overcome this low geometric probability, photometric transit surveys are designed to observe a large number of target stars simultaneously. The first successful projects for transit detection started at the beginning of the century, namely the Transatlantic Exoplanet Survey (TrES, Alonso et al. 2004), the Hungarian Automated Telescope (HATNet, HATSouth Bakos et al. 2004, 2013), Wide-Angle Search for Planets (WASP, Pollacco et al. 2006), and the Kilodegree Extremely Little Telescope (KELT, Pepper et al. 2007). These are ground-based surveys, which led to the discovery of hundreds of short-period ($P < 10$ days) exoplanets transiting bright stars.

The discoveries yielded by these missions, however, are mostly of hot giant planets, the so-called hot Jupiters (Fig. 1.2). This is because the Earth's atmosphere makes it hard to detect planets smaller than Neptune from the ground. Since the blocked flux (transit depth) is related to $(R_P/R_*)^2$, smaller planets can be detected from the ground if they orbit smaller, less bright stars (Fig. 1.1). Indeed, this was shown to be the case with two more ground-based searches focusing on M-dwarfs – MEarth (Nutzman & Charbonneau 2008; Irwin et al. 2015) and TRAPPIST (Gillon et al. 2011).

Small planets around hotter, including Sun-like, stars, however, still evaded detection. Space-based photometry came to the rescue with the launch of Convection, Rotation and planetary Transits (CoRoT, Baglin et al. 2006), which lead to the discovery of 34 planets. CoRoT was operational from 2006 to 2012 and perhaps its most notable discovery is CoRoT-7b – the first super-Earth with a measured radius.

The most productive mission to date, however, is the Kepler Space Telescope (KST). The nominal KST mission (Borucki et al. 2010), hereafter Kepler, was launched in 2009, prior to which only ~ 50 exoplanets were known. It observed 150,000 stars in the direction of the constellations Cygnus and Lyra continuously for four years. The discoveries made during this time made it possible to obtain information about the distribution and frequency of exoplanets and some key orbital and planetary parameters, thus allowing for the first statistical studies in exoplanet science to be conducted. The data showed that there are more planets than stars in our galaxy, that multi-planet systems are common, and often feature super-Earths and mini-Neptunes (Borucki 2017).

Unfortunately, by 2013 KST had lost two of its reaction wheels. The loss of the second one nearly put an end to the mission. Thankfully, a proposal adapting the “crippled” spacecraft to the new situation was accepted in 2014. This gave the beginning to the K2 mission (Howell et al. 2014), which utilised the same field of view (FOV) with high precision photometry as Kepler, but now with a different pointing strategy: the telescope began to monitor independent fields in the ecliptic plane. However, this rebirth came at the cost of a substantial noise increase resulting from complex spacecraft pointing adjustment manoeuvres necessitated by the loss of the reaction wheels.

The K2 fields were called campaigns and each lasted about 80 days. This meant that K2 would not be able to find long-period planets but it offered another advantage: the stars K2 observed were brighter than the ones in Kepler’s field. This made conducting radial velocity follow-up observations on K2 transiting candidates much more likely, and is the reason why, to this day, about 2100 of the planets from Kepler do not have mass estimates.

KST was retired when it ran out of fuel in 2018, yielding 2820 confirmed or validated exoplanets from Kepler and K2 combined⁷.

Currently, there are two ongoing exoplanet missions in space. The Transiting Exoplanet Survey Satellite (TESS, Ricker et al. 2015) and the CHaracterising ExOPlanet Satellite (CHEOPS, Benz et al. 2021). The primary mission of TESS ended in July, 2020 and is currently in its extended mission phase. Unlike the space-based surveys mentioned above, TESS has observed most of the sky since its launch in April 2018. This means that TESS observes

⁷2394 from Kepler and 426 from K2. Thousands more await confirmation. Data from <https://exoplanetarchive.ipac.caltech.edu/>

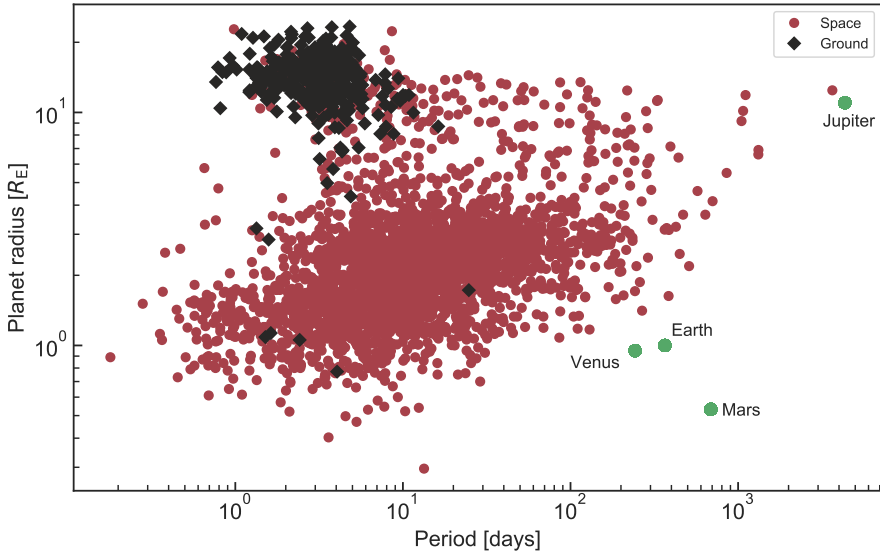


Figure 1.2: A period-radius plot of transiting planets detected from space (red) and from ground surveys (black). The sensitivity of ground-based surveys to short-period giant planets, i.e. hot Jupiters, is clear. The few small planets found using such surveys orbit small, faint stars.

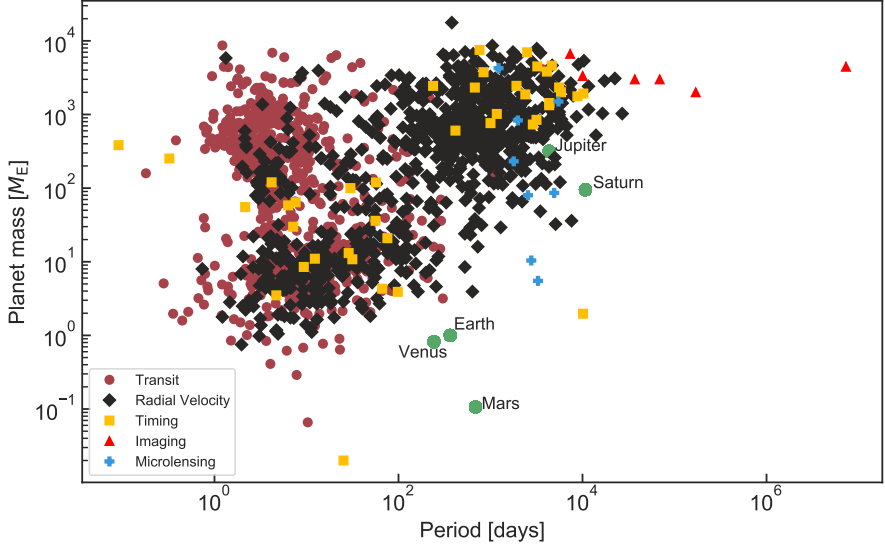


Figure 1.3: Period-mass plot of all planets with a mass estimate. A large number of the planets in the Fig. 1.2 are not found here due to the fact that many of the transiting planets were discovered by the Kepler mission, which observed stars too faint to follow-up with Doppler spectroscopy. The second thing clear from this plot is that cold Jupiters are in fact more common than the hot Jupiters (see text). It can also be seen that the planets detected via direct imaging are several AU away from their stars. Finally, as evident also in Fig. 1.2, the bottom right regions are nearly empty. This demonstrates the fact that our detection methods are not sensitive to small, long-period planets, such as planets in the habitable zones of Sun-like stars.

many bright stars, which will be easy to follow-up. Each field, however, is monitored for only about 28 days and thus will contain mostly short-period planets. Some of these may still be found in the habitable zones of their stars (i.e. where water can exist in liquid form), but those stars would then be low-mass ones. Nevertheless, TESS has so far led to the confirmation of over 100 new exoplanets, with thousands more in the works.

While CHEOPS (launched December, 2019) also employs the transit method, it differs from all of the above in the sense that its primary mission is to follow-up already known exoplanets around nearby bright stars, and improve the precision of their parameters. The highest priority planets are super-Earths up to Neptunes.

An upcoming mission with high hopes from the scientific community is PLANetary Transits and Oscillations (PLATO, Rauer et al. 2014) on track for a 2026 launch. As a transit survey mission, it will detect new planets around bright stars, with a focus on small planets in the habitable zones of Sun-like stars. It will have asteroseismology capabilities thanks to which we will obtain much lower uncertainties on the stellar parameters. Thus, PLATO will provide planet parameters of unprecedented precision, as well as the age of the planetary systems.

The radial velocity method

To describe the radial velocity (RV) method, it would help to recall Newton's third law: "for every action, there is an equal and opposite reaction". As is well known, planets (usually) orbit stars due to gravitational attraction, the strength of which is dictated by the masses of the bodies involved. In other words, just like planets are pulled on by their stars, so the stars are pulled on by the planets they are orbited by. This results in a scenario where a planet and a star orbit a point of equilibrium, their mutual center of mass, or barycenter, causing the star to wobble around this center of mass. Since we cannot directly see the planet, we can try and measure the line-of-sight (radial) component of the star's velocity. This is done by using a technique called Doppler spectroscopy which involves comparing the measured wavelengths of well-known spectral lines to the rest wavelengths of the same spectral lines measured in a laboratory. If the wavelengths are shifted towards the red end of the spectrum, corresponding to a positive RV, this indicates that the star is moving away from us; conversely, when the wavelengths are blue-shifted,

the RV is negative, meaning that the star is moving toward us (Fig. 1.4). The periodicity and magnitude of the RV can tell us if a planet orbits the star.

To detect the RV of a star induced by the presence of a planet, we need spectrographs with precision of about $0.01\text{--}100\text{ m s}^{-1}$ depending on the mass and period of the planet we are trying to detect. To illustrate, Jupiter induces a RV variation on Sun of 11.2 m s^{-1} at its distance of 5.2 AU ($P_{orb} = 11.9$ years). If Jupiter was instead in a 3-day orbit, similar to the early exoplanet discoveries, the corresponding RV amplitude would be $\sim 150\text{ m s}^{-1}$. Looking at the Earth, the RV in its current orbit is about 0.01 m s^{-1} which goes up to 0.6 m s^{-1} if we moved the Earth to an orbit of 1 day. The take-away from this example is that the RV method, like the transit method, is biased towards giant planets in short orbits, as evident from Fig. 1.3 because the induced RV variation is larger if the planet orbits closer to the star. A more in-depth explanation of the mechanics of this approach, as well as limitations and caveats, will be discussed in the next chapter.

To date (15/04/2021), the RV method is responsible for 837 exoplanet discoveries, including the first planet in orbit around a Sun-like star (Mayor & Queloz 1995). This planet was 51 Pegasi b (or 51 Peg b) – a Jupiter-mass planet in a 4.2-day orbit around the $1.1 M_{\odot}$ star, 51 Pegasi, in the constellation of Pegasus. Before this, there were a number of potential discoveries using the same technique which could not be verified at the time due to insufficient and suboptimal quality of the data. Some of those were later confirmed once additional data became available (e.g. Campbell et al. 1988; Latham et al. 1989; Hatzes & Cochran 1993).

As Fig. 1.3 shows, the majority of RV-detected planets are in the high-mass Jupiter range due to detection limitations inherent to the method. Since the early RV discoveries the precision of RV instrumentation, as well as data reduction and modelling techniques have been continuously improving, allowing for the mass determination of ever smaller planets at wider orbital separations. The lower end of the mass range in Fig. 1.3 exists thanks to second generation spectrographs with precision of $\sim 1\text{ m s}^{-1}$ like HARPS and HARPS-N (Mayor et al. 2003; Cosentino et al. 2012), and more recently ESPRESSO (Pepe et al. 2010, 2020) and EXPRES (Jurgenson et al. 2016), among others, which both reach the cm-level precision needed to detect Earth-like planets in Earth-like orbits.

As we have seen, the RV method has fallen behind the transit method

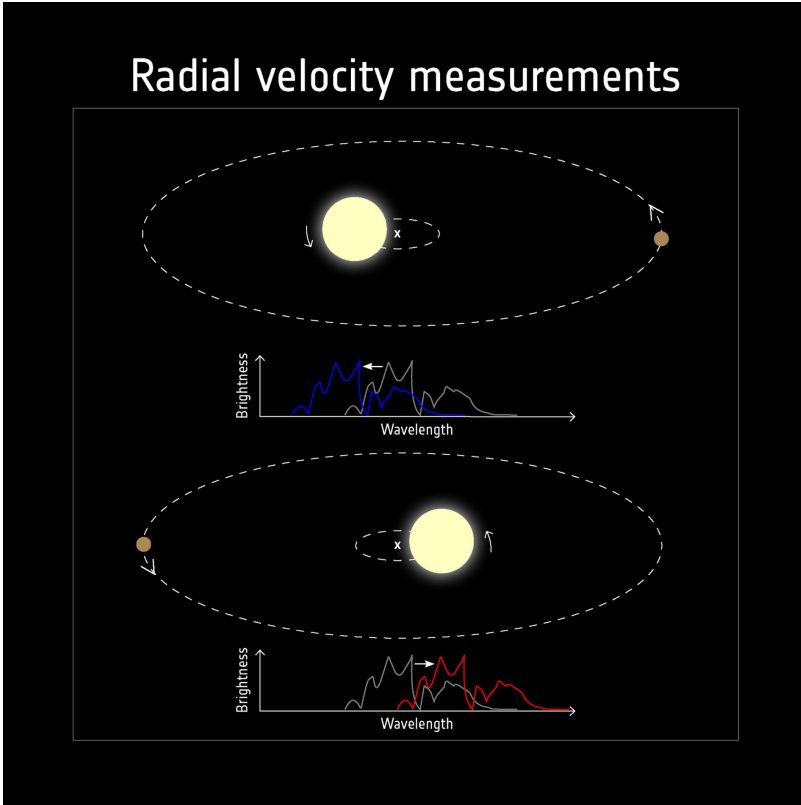


Figure 1.4: The Doppler shift of spectral lines. When the radial component of a star's motion is toward the observer, the spectral lines are blueshifted. Conversely, when the star moves away from the observer, the lines are redshifted. Image credit: ESA.

in terms of exoplanet yield. But what is, in fact, crucial here, is that the two methods go hand-in-hand. When the information derived from them is combined (planet radius from transits, and planet mass from RV), we are able to obtain an estimate of a planet’s bulk density, which in turn, allows us to begin to speculate about the structure and composition of exoplanets. However, the major difficulty in this effort is the fact that only about 20% of the planets with radii discovered to date have any kind of indication about their mass, with two-thirds of these being giant planets. Much fewer still, have uncertainties on their parameters low enough to allow characterisation.

1.3 Exoplanet demographics

Exoplanet demographics is an integral part of exoplanet science. It is intimately related to exoplanet characterisation and aims at understanding the distribution and frequency of exoplanets over a wide range of parameters and thus answering questions about planet formation and evolution.

As indicated for the first time by microlensing studies (Sumi et al. 2010), and soon after confirmed by results from both HARPS statistical surveys (Howard et al. 2010), as well as first results from the Kepler mission (Borucki et al. 2011), small planets ($< 4R_{\oplus}$), and in particular super-Earths and mini-Neptunes ($1 \lesssim R_{\oplus} \lesssim 4$, Petigura et al. 2013) are much more common than giant planets, especially with periods of < 50 days.

Another prominent result from the KST is the so-called radius gap – the apparent scarcity of planets in the 1.5 and $2 R_{\oplus}$ range (Fulton et al. 2017; Van Eylen et al. 2018, 2021), resulting in a bi-modal distribution of the $1 \lesssim R_{\oplus} \lesssim 4$ planets with $P_{orb} < 100$ days. Thus, two clear populations arise: the super-Earths of $1 \lesssim R_{\oplus} \lesssim 1.5$, and the mini-Neptunes of $2 \lesssim R_{\oplus} \lesssim 3$. Models suggest that for close-in planets with $a \lesssim 0.1$ AU this is likely due to XUV/X-ray photoevaporation – intense radiation from the host star causes mini-Neptunes to lose their envelopes in timescales of hundreds of \sim Myr, eventually leaving bare cores (Owen & Wu 2013; Lopez & Fortney 2014).

Another plausible mechanism which provides an explanation for the radius gap is core-powered mass loss (Ginzburg et al. 2016, 2018; Gupta & Schlichting 2019, 2020). In this case, this is due to a combination of stellar bolometric luminosity and a planet’s gravitational binding energy. The latter is converted into thermal energy during the planet’s accretion phase and is released out-

wards from the core and radiated away through the atmosphere, resulting in hydrodynamic escape. This theory produces similar observable demographic effects on the exoplanet population as photoevaporation. It is an active field of research (e.g., Rogers et al. 2021) and work on estimating the more dominant of the two effects and the scenarios in which each is more likely to prevail is ongoing.

A non-exhaustive list of other important findings, as summarised by Gaudi et al. (2020b), includes:

- the occurrence rate of giant planets around solar-type stars increases with distance from the host stars up until the snow line, after which point it starts to drop (Cumming et al. 2008);
- the frequency of giant planets which orbit at a distance smaller than ~ 2.5 AU, increases with stellar mass and metallicity (Fischer & Valenti 2005);
- the discovery of the hot Neptune desert – the apparent lack of exoplanets with masses $\sim 0.1 M_J$ and periods less than 2–4 days (Mazeh et al. 2016);
- "peas in a pod" - clustering of planets of similar sizes in planetary systems (Weiss et al. 2018);
- decreasing host star metallicity with the occurrence of small planets (Petigura et al. 2018)

In other words, as the above example show, there is a wealth of trends, some well-established, others so far only suspected, in places we did not expect to find any. Thus, the answers to many fundamental questions are, unfortunately, not yet within our grasp. We are still unable to give answers to questions like "How (un)common is our Solar system?" and "How common are planets in general?". The reasons for this are beyond enumeration but range between the biases due to the sensitivities of our detection methods, the reliability and representativeness of the current exoplanet census, insufficient information about the hosts, as well as the difficulty associated with combining the results from different surveys.

Nevertheless, the future is bright with promising current (TESS, CHEOPS, Gaia) and upcoming facilities, like the James Webb Space Telescope (JWST,

Beichman et al. 2014) and Atmospheric Remote-sensing Infrared Exoplanet Large-survey (ARIEL, Tinetti et al. 2021), which will allow us to improve our current understanding of exoplanet atmospheres. PLATO and the microlensing-utilising Nancy Grace Roman Space Telescope (Roman, Spergel et al. 2015), as well as exciting new direct imaging surveys, e.g. HabEx (Gaudi et al. 2020a), LUVOIR (The LUVOIR Team 2019), LIFE (Quanz 2019), on the other hand, will finally put planets in the most under-explored regions of parameter space and allow us to study them in unprecedented ways.

CHAPTER 2

A closer look at the theory behind transits and radial velocities

2.1 Orbital elements

In orbiting systems, all bodies are bound in orbits around a mutual center of mass called a barycenter. There are six fundamental orbital elements¹, which describe a Keplerian orbit. These are eccentricity, e ; the semi-major axis, a ; longitude of the ascending node, Ω ; argument of pericenter, ω ; inclination, i ; and true anomaly, ν . A schematic of such an orbit and its elements is shown in Fig. 2.1.

Ω , ω , ν and i are angles which describe the orientation of the orbit with respect to the reference frame, while a and e describe the size and shape of the orbit.

- e – the orbital eccentricity ranges between 0 and 1 for closed elliptical orbits, where a circular orbit corresponds to $e = 0$.
- a – the semi-major axis is half the major (long) axis of an ellipse. For a

¹Different texts differ slightly in which and/or the number of elements they present.

circular orbit, i.e. at $e = 0$, a is simply given by the radius of the circle.

- Ω – the longitude of the ascending node is measured in the reference plane and marks the angle between a reference line to the node at which the orbital plane crosses the reference plane and the orbiting body moves away from the observer.
- ω – the argument of pericenter is the angle between pericenter (where the orbiting body is closest to the barycenter) and the ascending node. ω is undefined for circular orbits and is assigned a value of $\pi/2$ in such cases.
- i – the inclination of the orbit with respect to the reference plane. $i = 0^\circ$ corresponds to a face-on orbital orientation, i.e. perpendicular to the plane of the sky.
- ν – the true anomaly is the angle between the position of the orbiting body and the pericenter and thus defines the body's location in the orbit at any given time.

2.2 Transit method

This section presents some theoretical background for the transit method. The information is not meant to be exhaustive and is to serve as a basic guide to the most crucial elements of this technique. More thorough descriptions can be found in texts from e.g. Seager & Mallén-Ornelas (2003) and Winn (2010).

Transit observables

There are four quantities that can be derived from photometric stellar time series (light curve) containing transits. As shown in Fig. 2.2, these are the period, P – the time between two consecutive transits, the transit depth, given by the amount of missing stellar flux during a transit; ΔF , the total transit duration between first and fourth contact points; t_T , and the transit duration between contact points 2 and 3; t_F , i.e. when the planet is fully contained in the stellar disc.

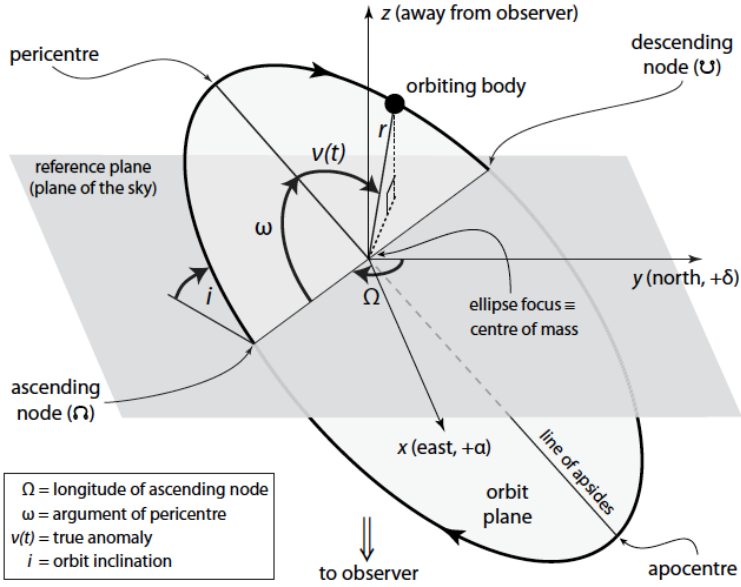


Figure 2.1: The mechanics of an elliptical orbit, including the six fundamental orbital elements: the semi-major axis, a ; eccentricity, e ; true anomaly, ν ; argument of pericenter, ω ; longitude of the ascending node, Ω ; and inclination, i . The reference plane represents the plane of the sky. Image credit: Perryman (2018).

If we assume that $M_p \ll M_*$, the period, P , together with the mass of the star (M_*), obtained via e.g. spectroscopic observations and stellar modelling, can give us the semi-major axis of the orbiting body using Kepler's third law:

$$a \simeq \left(GM_* \left(\frac{P}{2\pi} \right)^2 \right)^{1/3} \quad (2.1)$$

The amount of light periodically blocked when an opaque object passes in front of a star, or the ratio of flux observed during a transit, ΔF , to the flux with no transit, F , gives the squared planet to star radius ratio:

$$\frac{\Delta F}{F} \simeq \left(\frac{R_p}{R_*} \right)^2 \quad (2.2)$$

For brevity, the ratio $\Delta F/F$ will hereafter be referred to as ΔF . This equation also illustrates the fact that solely from the missing flux, we only know the planet radius relative to stellar radius, thus highlighting the importance of knowing the host star well.

The transit duration represents the fraction of the period during which the sum of the radii of star and planet is greater than the projected distance between the center of the two bodies. Adapted from Seager & Mallén-Ornelas (2003), this can be expressed in the following way:

$$t_T = \frac{P}{\pi} \arcsin \left(\frac{R_*}{a} \left\{ \frac{[1 + (R_p/R_*)]^2 - b^2}{1 - \cos^2 i} \right\}^{1/2} \right) \quad (2.3)$$

The form of this equation can be further simplified by defining the impact parameter, b , as $b = a \cos i / R_*$, which for the case of a planet in a circular orbit passing through the middle of the stellar disc is set to zero, since $\cos i = 0$, when $i = 90^\circ$. In addition, if R_* and thus R_p are known, as per Perryman (2018), eq. 2.3 then becomes:

$$t_T \simeq 13 \left(\frac{M_*}{M_\odot} \right)^{-1/2} \left(\frac{a}{1\text{AU}} \right)^{1/2} \left(\frac{R_*}{R_\odot} \right) \text{ hours} \quad (2.4)$$

This translates to ~ 25 hours for a planet at the distance of Jupiter, and ~ 13 hours at the distance of Earth.

The geometry of a transit, together with the aforementioned parameters, is

illustrated in Fig. 2.2.

Other physical quantities

The stellar density, ρ_\star , is an important parameter that can be used diagnostically to test if the value obtained from the transit light curve is consistent with the spectroscopically derived one. Alternatively, in the absence of a reliable spectroscopic estimate, a high signal-to-noise transit light curve can be used to derive a value for ρ_\star . If the value suggests a giant host star, depending on the fraction of missing flux, the transiting companion can be discarded as a less interesting (from a planet hunting perspective) massive body.

Assuming the planet is much smaller and less massive than the host star, the stellar density, ρ_\star , can be calculated as:

$$\rho_\star \approx \frac{3\pi}{G} \frac{1}{P^2} \left(\frac{a}{R_\star} \right)^3 \quad (2.5)$$

If, on the other hand, the stellar parameters are well constrained and known to be reliable, an alternative equation taking into account t_F and t_T can be used to estimate the period in the cases of suspected single transit events (see Perryman 2018).

Another useful quantity that can be calculated solely from transit photometry is the planet's equilibrium temperature, T_{eq} . If the stellar effective temperature, T_{eff} , is known either through spectral classification tables or stellar models, A is the planet's albedo², and assuming isotropic planetary emission, then:

$$T_{eq} = T_{eff}(1 - A)^{1/4} \sqrt{\frac{R_\star}{2a}} \quad (2.6)$$

Finally, the insolation received at the planet, F_P , can be calculated via the following expression:

$$F_P = \left(\frac{R_\star}{R_\odot} \right)^2 \left(\frac{T_{eff}}{T_\odot} \right)^4 \left(\frac{\text{AU}}{a} \right)^2 F_\oplus, \quad (2.7)$$

where R_\odot and T_\odot are the radius and effective temperature of the Sun, and

²The portion of the incident stellar radiation on a body that is reflected back out into space.

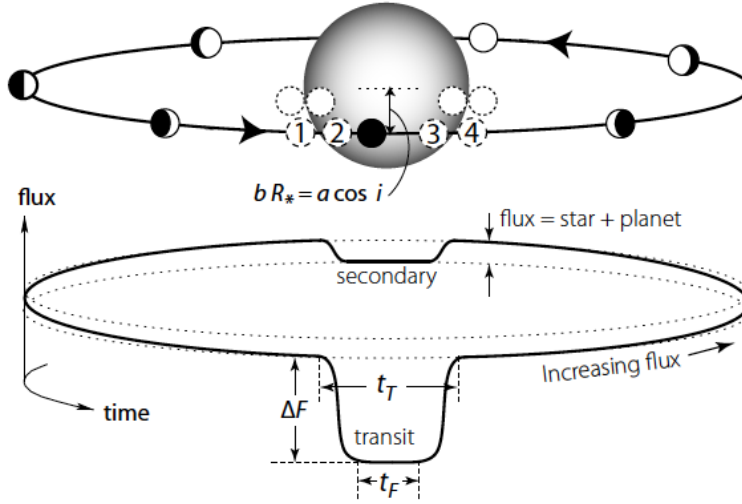


Figure 2.2: Diagram illustrating the mechanics of transits and occultations. Contact points 1-2 correspond to the planet ingress, while points 3-4 – to the egress. The total transit duration, t_T , is between points 1 and 4, while t_F is between 2 and 3. The impact parameter, b , is 0 if the planet transits straight through the middle of the star, corresponding to the longest transit duration and steepest transit flanks. b grows up to a maximum value of 1 the farther from the middle of the stellar disc a planet transits. The least amount of flux is received during a transit, and the genuine stellar flux is recorded during the secondary eclipse, i.e. when the planet goes behind the star. During the rest of the orbit, the planet shows different amounts of its face as it is illuminated by the star, reaching a maximum total flux just before it goes behind the star, when its face is fully illuminated. Image credit: Perryman (2018).

F_{\oplus} is the insolation received at Earth.

Challenges and caveats

Limb darkening

Limb darkening is the phenomenon which causes stars to appear brighter towards the middle of the disc and darker (redder) towards the edge (limb). When an observer looks straight on towards the centre of a stellar disc, the angle of the line of sight to the center of the disc is zero. However, looking towards the limb of a star, this angle increases, and the observer is only able to see into shallower layers of the stellar atmosphere, as compared to looking at the center. Because deeper layers are generally hotter than shallow layers, photons from the limb appear redder and photons originating from areas closer to the centre appear bluer.

The effect limb darkening has on transits is that it causes real transits to have rounded bottoms, as opposed to flat bottoms if considering a uniform stellar disc. This blurs the distinction between the different contact points (Fig. 2.2), most prominently affecting the impact parameter, b , and thus misinterpreting the transit depth and other parameters.

There are a number of limb darkening laws³ that have been developed by different authors in an attempt to account for this effect. Perhaps the most popular one, which balances computational time and complexity, is the quadratic law.

For a more detailed discussion regarding limb darkening in the context of transits, see e.g. Mandel & Agol (2002).

Stellar activity in light curves

Stellar activity, and most notably starspots, can also affect the transit depth, and thus the estimate of the planet radius.

Two cases are worth mentioning in this context, as discussed in Pont et al. (2008). The first is when the star is spotted and the transit chord passes through the spots. In the cases of very clear transits, for e.g. large planets around bright stars, a bump in flux can be seen when a transiting planet crosses a spot. However, in most cases, the signal-to-noise ratio and/or the

³It is worth noting that the limb darkening laws are not really "laws" in the full sense of the word, but rather fitting formulas.

observing cadence of the light curve are insufficient to allow for this to be recognised. Thus, the observer is unaware that the radius of the planet may be underestimated due to the planet blocking a smaller portion of the overall flux.

The second case is when the star is heavily spotted but the planet does not cross any of the spotted regions. This scenario has the opposite effect: the planet radius is overestimated because the planet blocks a bright, unspotted region of the stellar disc, which in turn contributes a larger fraction of the total flux as compared to spotted regions.

Nevertheless, starspots have an important role in understanding the rotation and differential rotation of stars, and in the cases when a transiting planet crosses a spot, it may be possible to derive information about the stellar obliquity with respect to the planet's orbit (Sanchis-Ojeda et al. 2013).

Sources of false positive transit detections

The secondary eclipse, or occultation, as illustrated in Fig. 2.2, can be used as an important diagnostic tool to help avoid misidentifying a transiting companion as a planet. As described by Collier Cameron (2016), only the largest and most irradiated planets can produce occultations visible in a light curve, and the larger the eclipsing body, the larger the occultation. Similar to the depth of a transit, a light curve with a very prominent secondary dip often means that the eclipsing body is likely self-luminous, thus pointing to an eclipsing binary⁴ (EB) scenario. Usually it is easy to distinguish between a planetary transit and a transit of a smaller, less bright star because the depth of the latter would be much higher than the former. Sometimes, however, a bright background star, not necessarily physically bound to the EB, can add to the total flux received from the target, diluting the transit event and causing it to appear shallower, concealing the non-planetary nature of the transit source. Alternatively, a grazing EB with stars of similar mass will produce a small dip in brightness, which can be mistaken for a planetary transit. In such a scenario the occulted area would be much smaller than the area of the occulting object. Another possible scenario is when a small dim star transits in front of a larger, brighter star. Since Jupiter is the size of a late-type M-dwarf, $\sim 0.1 M_{\odot}$, the transit depth caused by such a star transiting a Sun-like star may easily be mistaken for a Jupiter-sized planet.

⁴An eclipsing binary is a system of two stars orbiting each other.

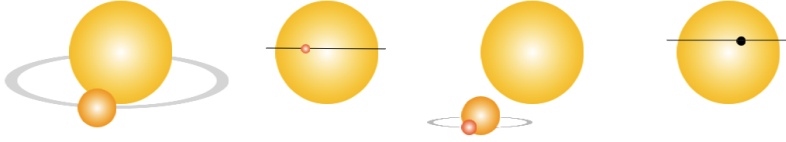


Figure 2.3: Four possible scenarios which could cause a transit-like feature. From left to right: a grazing stellar binary, a red dwarf transiting a star that is much larger, a blended eclipsing binary, a genuine transiting planet. For more details, see text.

These are some typical examples of false-positive detections. Luckily, there are tests that are employed by pipelines to reveal these scenarios. Some common examples are the even-odd transit depth, where a significant difference between even and odd transit depths and durations could point to an EB; the photocenter in and out of transit shift test checks if the target star is the true transit source. Alternatively, follow-up photometric adaptive optics observations (e.g. Ciardi et al. 2015), as well as observations at different wavelengths (e.g. Parviainen et al. 2019), can be performed to rule out false positive scenarios.

2.3 Radial velocity method

As briefly described in Sect. 1.2, all the bodies in an orbital system orbit the barycenter, including the central body. In the RV case, the body of interest is the star, which executes a Keplerian orbit around the barycenter, and can be described by Fig. 2.1. The line-of-sight (radial) component of the orbital velocity, i.e. the **radial velocity**, v_r of the star is given by

$$v_r = v_z + K[\cos(\omega + v) + e \cos \omega], \quad (2.8)$$

where v_z is the systemic velocity, i.e. the radial component of the proper motion of the barycenter with respect to the observer, and K is the **radial velocity semi-amplitude**,

$$K = \left(\frac{2\pi G}{M_\star^2 P} \right)^{1/3} \frac{M_p \sin i}{\sqrt{1 - e^2}} \quad (2.9)$$

This is the case for a two-body system. It is common, however, that planets are found in multi-planet systems. In such a case, the star is still the gravitationally dominating body and the interaction between the relatively low-mass planets can be neglected. To solve for the Keplerian orbit of each planet, we would then have

$$v_r = v_z + \sum_{i=1}^N K_i [\cos(\nu_i + \omega_i) + e_i \cos \omega_i], \quad (2.10)$$

where N is the number of planets, and each planet i has its own set of parameters.

The uncertainties in M_p are generally dominated by the noise of the dataset, which also dictates the precision of P and K . If the star is not well understood so that the stellar parameters are not well-constrained, the uncertainty in M_\star can further deteriorate the precision of M_p .

Furthermore, from eq. 2.9 we can see that K scales linearly with M_p but is inversely proportional to both $P^{1/3}$ and $M_\star^{2/3}$. This explains why longer-period planets induce a smaller K to more massive stars, which also demonstrates why the first planets to be found were indeed close-in giant planets.

Combining the two methods

A RV timeseries can give information about P , K and e . Estimating the planetary mass, M_p , however, depends on the inclination, i (eq. 2.9), which cannot be found from RV data. This, and the fact that most planets are not transiting, is why the majority of RV-discovered planets only have an $M_p \sin i$ estimate, i.e. the planet's minimum mass. The i can, however, be found from transit observations via the impact parameter, b , as mentioned in the previous section.

Here, it is worth reiterating that combining the planet radius and inclination from transits with the minimum mass from RV observations gives us the planet's bulk density, which allows us to perform a first-step planet characterisation. By comparing the position of the planet on a mass-radius diagram with composition models, we can speculate about the planet's composition

and internal structure.

Finally, with the two methods together, we are able to extract the following important parameters: T_0 (the mid-transit time), P , e , ω , R_p/R_\star , a/R_\star , i , and K . These can help us derive one more physical parameter, the planet's surface gravity, g_p . Originally from Southworth et al. (2007):

$$g_p \equiv \frac{GM_p}{R_p^2} = \frac{2\pi}{P} \frac{\sqrt{1-e^2}K}{R_p^2/a^2 \sin i} \quad (2.11)$$

In the not-so-rare cases when we do not know the host star as well as needed, the right side of this equation allows us to eliminate the dependence on the stellar parameters and thus avoid any uncertainty associated with them. It is also worth noting that, since R_\star , unlike M_\star , can be determined with good accuracy, the planet's bulk density can be found by combining g_p and R_\star (Rodríguez Martínez et al. 2021).

Alternatively, we can use the standard equation for Newton's law of universal gravitation, i.e. the middle part of eq. 2.11, in the cases when we do have information about the star, and compare the two estimates for g_p as a sanity check.

Challenges

RVs are measured by comparing the wavelengths of Doppler-shifted spectral features of a stellar photosphere to the rest wavelengths of said features, λ_0 , such that

$$\frac{\Delta\lambda}{\lambda_0} = \frac{v_r}{c}, \quad (2.12)$$

where $\Delta\lambda$ is the difference between the shifted and rest wavelengths of a spectral line, and c is the speed of light. In practice this is done by comparing an observed spectrum with a template spectrum, where the latter is shifted in velocity space so that it matches the former. The better the correlation between the spectra, i.e. the more features that can be precisely matched between the two spectra, the better the achieved RV precision.

This leads us to the first challenge.

Spectral lines strength

For the above process to be successful, the star must have prominent spectral features. Hotter, and thus more massive stars, have fewer, broader and shallower spectral lines since the number and depth of spectral lines decrease with increasing T_{eff} . Stars with a high rotational period, i.e. fast rotators, are also difficult to study due to rotational broadening of the lines. This is caused by the redshifting of the light from the star's receding hemisphere, while the light from the approaching hemisphere is blueshifted. Finding the position of the centroid makes the detection of Doppler shifts in such lines challenging. In contrast, cooler, metal-rich⁵ stars produce many deep and narrow lines, which are much easier to study (Hatzes 2016).

Activity in spectroscopic data

As in the case with photometric surveys, stellar spectroscopy is also significantly affected by different sorts of stellar activity, also referred to as stellar jitter. There are variable sources for this activity, which are driven by processes taking place in different regions of stars. Stellar activity is the biggest nuisance in the search particularly for sub-Neptune-sized planets since it can conceal or even emulate the weaker planet-induced signals. I outline some common groups of activity sources following Dumusque et al. (2011).

Granulation of the stellar surface (for stars with convective shells) is caused by convection in the star's outer layers. These can have lifetimes of minutes to a few days, depending on the size of the granules. This is a pattern familiar from the surface of the Sun and is caused by hot, bright parcels (the granules) rising to the top, surrounded by darker regions where the gas has cooled, sinking back into the interior. The effect is that the stellar surface is dominated by the granules, which move toward the observer, resulting in a net convective blueshift. The RV jitter caused by this effect depends on the size of the granules.

Stellar oscillations represent vibrations or pulses in brightness caused by pressure waves in the stellar interior rebounding at the surface. This phenomenon lasts for a few tens of minutes (Bedding et al. 2001).

Both granulation and oscillations cause an RV jitter of a few m s^{-1} and can

⁵In astronomy, elements different from hydrogen and helium are referred to as metals.

be mitigated by employing a suitable observing strategy (Dumusque et al. 2011).

Stellar jitter is, however, dominated by active surface regions such as starspots, plages and faculae⁶. These are magnetically driven, with field lines inhibiting the convection process, thus preventing these regions from manifesting the aforementioned net blueshift. As a result, the overall stellar RV will vary with stellar rotation as these features rotate in and out of view. As expected, the amplitude of the RV variation resulting from active surface regions changes during a stellar activity cycle. As shown by Meunier et al. (2010), in the case of the Sun this is 40 cm s^{-1} during solar minimum, and 140 cm s^{-1} during solar maximum. This is expected to be similar for Sun-like stars, but late type stars, like cool K and M dwarfs, tend to be more magnetically active (e.g., Reiners et al. 2010; Andersen & Korhonen 2015) and the aforementioned values are expected to be higher.

⁶Spots are cooler, while plages and faculae are hotter than their surroundings.

CHAPTER 3

From photons to worlds

3.1 Finding transits in light curve data

A major setback in exoplanet detection is the presence of systematics (red noise) in the timeseries photometry. This noise has an instrumental and spacecraft environment-related origin and is very much a factor in the exoplanet detection effort. Well-established data preprocessing pipelines developed by the Kepler and TESS teams, as well as alternatives provided by the community, generate stellar light curves with common instrumental systematics as well as dilution from nearby sources removed (Smith et al. 2012; Stumpe et al. 2012; Jenkins et al. 2016). These light curves go through rigorous and multi-stage testing before they are made available to the public and are in most cases of optimal quality. One can, however, also extract their own light curves from the raw pixel data using simple aperture photometry¹, using a custom aperture. This may be required in cases when the default option is not the optimal one, e.g. in crowded fields, or a bright companion contributing flux to the aperture. The so extracted custom light curves can then be detrended

¹Aperture photometry is the summing up all the pixel values as a function of time in a specific aperture.

using a variety of techniques.

While red noise is generally taken care of at the preprocessing stage, the light curves still contain stellar activity of the periodic and aperiodic kind, in the form of brightness variations and stellar surface structures. This is useful in the cases when the nature of the stellar activity is of interest, e.g. when the stellar rotation period is identifiable and thus easy to determine. However, this is only considered a nuisance signal when trying to extract the signals corresponding to any transiting planets. Adverse effects resulting from stellar rotation, eruption events, star spots, pulsations, among others, together with the actual light curve precision achieved, are the main reasons for missing small planets. The "temper" of the star, thus, presents a significant challenge, and a substantial effort in accounting for it has been put in through the years since the first transit detection by Charbonneau et al. (2009). Techniques involve detrending using the Savitzky-Golay high-pass filter (Savitzky & Golay 1964), polynomial (Gautier et al. 2012) or median filter (Tal-Or et al. 2013), wavelets (e.g., Jenkins et al. 2010), or Gaussian process (GP) regression (e.g., Aigrain et al. 2015), among others.

Once all the signals which are not of interest to the transit hunter are removed, it is time to move on to the core goal of light curve analysis. In terms of exoplanets, this is to detect new planets and analyse the size and shape of an exoplanet transit in order to obtain the candidate's radius and orbital period. Due to different scenarios that can cause a false positive detection (Sect. 2.2), combined with the low probability of a transit actually occurring, thousands of light curves need to be studied for every genuine planet. Based on these constraints, to find the needle in the haystack, we utilise transit detection algorithms (TDAs), the most well-known and commonly used of which being the box-fitting least squares (BLS) algorithm (Kovács et al. 2002). The main premise is that a transit event is a steep and shallow dip with a short duration, which thus appears boxlike. BLS phasefolds the light curve at a wide range of periods and extracts the boxlike event by fitting a square box to the phase range. The period which delivers the lowest χ^2 is selected as the correct one. There is an abundance of literature on the topic, however, and a wide selection of TDAs exists, some based on or related to BLS (e.g., Renner et al. 2008; Grziwa et al. 2012). Others do not: e.g. Cabrera et al. (2012) use a second order polynomial to approximate the transit shape, while Hippke & Heller (2019) use a transit-like search function, taking into account limb darkening

and ingress and egress. Many TDAs are complete packages and include light curve detrending and frequency filtering or transit masking to facilitate the search for additional companions.

TDAs do not or cannot reliably test for the different astrophysical false-positive scenarios. Therefore, the final step is the visual examination of the transit events that passed all tests. These include checking for the difference between even and odd transits, the presence of secondary eclipses, the depth and shape of the transits and the overall consistency between the parameters.

Alternatively, algorithms capable of distinguishing between false positives and genuine planetary transits (Fig. 2.3) can also be used. A number of these have been developed through the years, e.g. *VESPA*, (Morton 2012), *PASTIS*, (Díaz et al. 2014), *TRICERATOPS*, (Giacalone et al. 2021), originally motivated by the need to validate the many Kepler planets too faint for RV follow-up. Many of the planets known to date have been validated using these techniques.

To illustrate, I show in Fig. 3.1 the light curve of K2-99, which reveals a Jupiter-size planet in an 18.25-day orbit around a relatively bright ($V_{mag} = 11.1$) subgiant² star, as reported by Smith et al. (2017). The light curve presented here (grey dots in Fig. 3.1) is from K2’s sixth observing field, or campaign³, and was systematics-removed by the pipeline developed by Vanderburg & Johnson (2014), which became the most widely-used one for the two-wheeled K2 mission. The four transits of K2-99b are easily identifiable by eye. The star is relatively quiet, manifesting clear long-term variability, which is easy to remove by any of the traditional methods mentioned above. In this case, and analogous to Paper A (Sect. 5.2, Georgieva et al. 2021), we used GP regression⁴ to identify the best-fitting model to the data (red curve) and subtracted it from the original light curve (grey dots) to obtain the detrended one (blue dots).

²A subgiant is a star that is brighter than a star of the same spectral class and has begun the final stages of its life.

³This target was observed again in Campaign 17, which is not included in this example.

⁴The light curve was detrended using the Python package *citlalicue*, available at <https://github.com/oscaribv/citlalicue>.

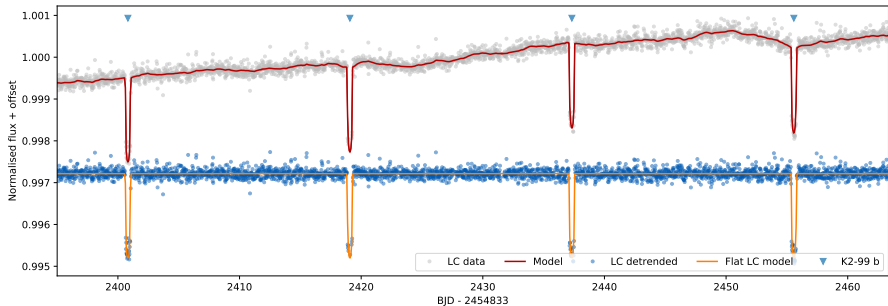


Figure 3.1: K2-99 Campaign 6 light curve by Vanderburg & Johnson (2014) in grey with GP and transits overplotted in red, and resulting detrended light curve in blue. Individual transits of the Jupiter-size planet k2-99b are marked with blue triangles.

3.2 Joint modelling of transits and RVs

As mentioned in Chapter 1, by combining transit photometry with RV measurements, we can measure a planet’s true mass and determine its mean density. As further shown in Chapter 2, RV and light curves are described by time-dependent parametric equations. These can be compared to models to help infer a planetary system’s parameters. This is typically done by using Bayesian model-fitting techniques. The value of Bayesian statistics is in its power to formulate a framework for providing quantitative answers to inverted questions such as the probability of a set of events explaining an observed outcome. This approach is well suited for the problems of exoplanet characterisation since it allows us to infer parameters which we cannot observe directly due to the nature of transit and RV observations.

Still, posing such a problem in a Bayesian way is by itself only half of the story. Solving it involves computing the probability distribution that a set of parameters explain a given set of data. Since this cannot be solved analytically in all but the simplest cases, one convenient and popular solution to such a numerically demanding problem is provided by the Markov Chain Monte Carlo (MCMC) method (Metropolis et al. 1953; Hastings 1970). MCMC has become an essential tool for data analysis and has been steadily growing in popularity in the astronomical community. To determine the physical parameters of an exoplanet system we turn to this reliable approach for the simultaneous mod-

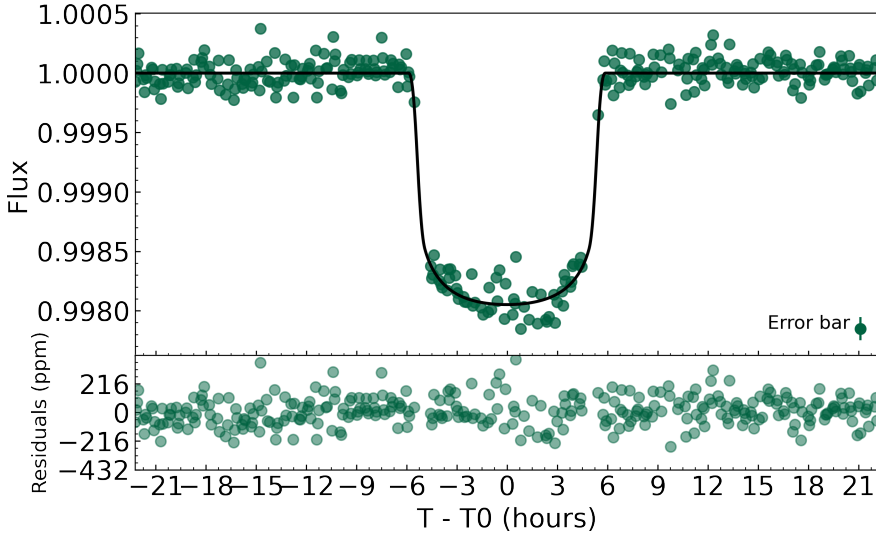


Figure 3.2: K2-99 light curve with residuals phasefolded to the orbital period of K2-99b. The black curve is the best-fitting transit model.

elling of transit photometry and RV data, using the code `pyaneti` (Barragán et al. 2019a).

The continued story of the K2-99 system can be followed in the below figures. The deep phasefolded transit with the best-fitting model shown in Fig. 3.2 yields a radius of $1.26 \pm 0.05 R_J$. The RVs yield a semi-amplitude of $K = 55 \pm 4 \text{ m s}^{-1}$, which combined with an inclination of $i = 88.5_{-1.5}^{+1.0}$ degrees, gives $M = 0.95 \pm 0.08 M_J$. What is interesting to notice from Fig. 3.3 that is not evident from the light curve in Fig. 3.1, is that the planet has an eccentric orbit, corresponding to $e = 0.2_{-0.04}^{+0.06}$. But perhaps the most intriguing part is the negative linear trend in the RV timeseries (top panel): what this trend indicates is the presence of an outer companion with unconstrained parameters. Additional observations can, of course, reveal the nature of K2-99b’s distant neighbour.

A more detailed description of the system can be found in Smith et al. (2017).

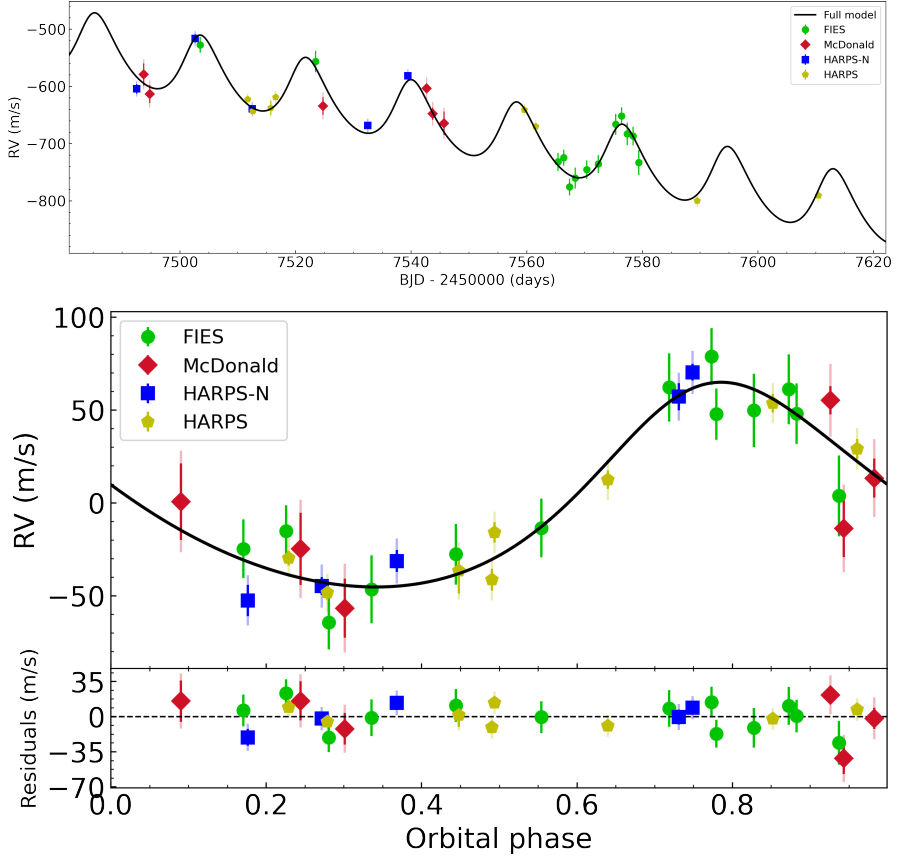


Figure 3.3: Top: K2-99 RV timeseries. The different colour markers represent data from the different instruments. The black curve is the RV planet model. A clear downward linear trend is visible, indicative of the presence of another planet in a wider orbit. Bottom: RV data folded on the orbital period of K2-99b, again with solid black curve representing the best-fitting model. Both plots show the eccentric nature of this planet’s orbit. The deviation from a sinusoid (i.e. circular orbit) evident in both panels is the signature of an eccentric orbit, in this case corresponding to $e = 0.2$.

The harsh reality

The K2-99 system presented above is, unfortunately, only a rare example of a straight-forward solution, for which Kepler’s laws of planetary motion and Newton’s laws of universal gravitation work beautifully. The mass and radius of K2-99b reported in the previous section correspond to a precision of $\sim 4\%$ and 8.4% , respectively. Of the 4375 discovered planets, 113 of them boast such precision, of which only 12 are small planets ($< 4R_{\oplus}$). This is symptomatic of the challenges described in the previous chapter. Even with the most precise spectrographs currently available, such as EXPRES and ESPRESSO, with their recently reached 58 cm s^{-1} (Brewer et al. 2020) and 30 cm s^{-1} (Suárez Mascareño et al. 2020), respectively, the ability of RV surveys to detect and characterise small planets is still limited by stellar activity. In the more complex cases when the stochastic nature of stellar photospheric variability is evident in the signal, such as the case of the TOI-1260 system (Chapter 4, Georgieva et al. 2021), to obtain a planetary solution we must employ more sophisticated strategies.

Magnetically-driven stellar variability produces time-varying distortions in the spectral line profiles of stars. These lead to systematic errors, which reduce the spectroscopic measurements’ precision, limiting the ability to measure the masses of both newly-discovered and known low-mass exoplanets. This is particularly true for planets with orbital periods of a few tens of days and higher (Collier Cameron et al. 2020). But depending on the variability of the star and the time-sampling of the data, shorter period planets can be affected by either being missed or reaching too low mass precision to afford characterisation.

Stellar activity has traditionally often been accounted for by modelling it as one or multiple sinusoids at the star’s rotation period or one of its harmonics (Queloz et al. 2009; Boisse et al. 2011). While in many cases this is a sufficient approach, in others it can be too simplistic and lead to spurious detections (see e.g., Rajpaul et al. 2016), since it does not take into account the temporal evolution of active regions and assumes the removed signals are periodic and long-lasting.

Recently, several strategies aiming at dealing with stellar activity mitigation for the more complex cases have been put forward. Photospheric temperature and pressure affect atomic transitions differently, so individual spectral lines are affected by activity to a different extent (Davis et al. 2017). Tak-

ing advantage of this, Dumusque (2018) demonstrated that deriving line by line RVs in this way, as opposed to the traditional approach using the cross-correlation function (CCF) between the observed and the template spectrum (see Sect. 2.3), can mitigate photospheric-induced RVs and thus account for the nuisance activity signal. The possibility to remove activity signals solely by identifying changes in the spectral line shapes using machine learning techniques was demonstrated by de Beurs et al. (2020), while Collier Cameron et al. (2020), on the other hand, propose a complex algorithm which makes use of the RVs derived from the CCF between an observed spectrum and a digital mask. All of these are novel methods and are active fields of research. The latter two have been tested on simulated data as well as data of the solar spectrum, and show great promise for future applications to exoplanets.

Until approaches such as these gain enough traction, however, we rely on stochastic modelling techniques like GP regression (e.g., Haywood et al. 2014), which has gained popularity in recent years. The GP is an infinite-dimensional generalisation of the familiar Gaussian distribution. In conjunction with a Bayesian formulation, it can be utilised for building flexible non-parametric models. This flexibility generally makes them look like they can fit any data well, which can be misleading. Therefore, it is useful to inform the GP and constrain said flexibility by adding any available information about the system. As put forward by Rajpaul et al. (2015), additional data such as ancillary RV-contemporaneous activity indicator timeseries can become useful. Activity indicators, as their name implies, are sensitive to stellar activity only, making them uniquely suited for decorrelating this activity from RV data in the effort of disentangling the genuine planetary signal(s), as done by e.g. Mayo et al. (2018); Barragán et al. (2019b).

This is the very approach used to obtain the best possible accuracy of the planets in the TOI-1260 system, the basis for this work (Georgieva et al. 2021).

CHAPTER 4

Paper summary

4.1 Paper A

In this paper we present the detection and characterisation of two short-period mini-Neptunes in the $2\text{--}3 R_{\oplus}$ range orbiting the late K-type star TOI-1260. The transit detections were based on photometry from TESS observing sectors 14 and 21. TOI-1260b is the inner planet with a radius of $\approx 2.3 R_{\oplus}$ and period of 3.13 days. TOI-1260c is its outer neighbour, with a radius of $\approx 2.8 R_{\oplus}$ and period of 7.49 days. Subsequent follow-up Doppler measurements with HARPS-N allowed us to make a 6-sigma detection for the mass of planet b, yielding $M_b \approx 8.6 M_{\oplus}$ and a 3.6-sigma detection on the mass of planet c, $M_c \approx 11.8 M_{\oplus}$. Follow-up ground based photometry excluded the possibility of a contaminating source, both as a nearby binary companion, and as a diluting source.

The star exhibits a complex variability pattern, the effects of which we removed from the TESS light curves using a GP. For the spectroscopic measurements, said pattern could not be modelled effectively using a trivial sinusoid fitting approach. Thus, to disentangle the planetary signals from the stellar variability-induced signal present in the data, we again used GP regression. In

this latter case, we modelled the RVs alongside the timeseries of the S-index activity indicator. This is the so-called multi-dimensional GP. The S-index is an indicator for chromospheric activity and is based on the strength of the core reversal of the Ca II H and K lines. Thus, it is solely sensitive to the stellar activity portion of the signal and served to constrain and separate the activity-induced signal from the RV, leaving only the part of the signal caused by the planets.

As previously stated, the radius gap unravels two distinct populations. While planets with radii smaller than about $1.8 R_{\oplus}$ are well consistent with an Earth-like composition (iron and silicate rock), the composition of mini-Neptunes, particularly in the region $2\text{--}3 R_{\oplus}$, is still somewhat of a mystery. These types of planets are not found in the Solar system. Based on the parameters with their associated uncertainties that we obtain from the modelling, in the absence of additional data (e.g. transit spectroscopy) the only way we can try to learn about the possible compositions and structures of these planets is by simulations. We thus decided to perform simulations of temporal atmospheric escape under photoevaporation to allow us to speculate about the possible compositions of the two TOI-1260 planets. Assuming the presence of a primordial hydrogen/helium atmosphere for both planets, we found that planet b is unlikely to have retained it. However, being in a highly irradiated orbit, planet b is possibly a water-rich planet, featuring a thick steam atmosphere. This could mean that the planet is in fact a dense, rocky core with an expansive atmosphere, inflating its radius. On the other hand, we find that planet c may have retained such a primordial atmosphere throughout its evolution.

Another interesting result is that we uncovered the likely presence of a third planet, external to the other two. The transit of this planet is not visible in sector 14, and its existence was initially only hinted at by a single transit event visible in sector 21. Further analysis of the light curve data of sector 21 showed that a second transit of this tentative planet is possibly overlapping with a transit of planet c. We performed a multi-transit analysis of this simultaneous event, and found that this scenario explains the data better. If this outer planet is real, it would have a radius of $\sim 2.75 R_{\oplus}$ and a period of 16.6 days, making it a warm mini-Neptune. Such a period puts a transit of this planet in the spacecraft downlink time interval in sector 14, explaining the ab-

sence of this planet in the light curve for that sector. Furthermore, this orbital period corresponds to about half the rotation period of the star that our GP analysis helped us find. Given our relatively short and sub-optimally sampled RV dataset, despite our best efforts, we could not claim a solid confirmation of planet d since the precision of the mass detection we reached was less than 2-sigma. Follow-up observations will confirm or refute the existence of this planet. Interestingly, if TOI-1260 is indeed confirmed to have (at least) three planets, their radii would make the system a perfect example of the "peas in a pod" scenario.

TOI-1260 is a good example of the challenges associated with both transit detection and mass determination via Doppler spectroscopy due to the presence of stellar activity of stochastic nature in both the TESS transit and HARPS-N RV data for this target. This necessitated the use of advanced methods to ensure the highest possible precision for the planet parameters, given the limitations of the datasets. In addition, the ambiguity of the planet compositions warranted the modelling of their respective temporal atmospheric evolutions.

Furthermore, performing additional observations and thorough analyses on mini-Neptunes, can help to find out if mini-Neptunes may in fact be super-Earths with inflated radii (Turbet et al. 2020) – an idea that has been growing in popularity in the field. Finally, we must not forget the critical importance of a well-characterised host star, without which none of the aforementioned discoveries and analyses would have been possible.

CHAPTER 5

Outlook

5.1 Concluding remarks

From the first protoplanetary disk to ever be observed in 1984, through the early discoveries in the 1990s of a planet around a pulsar (Wolszczan & Frail 1992) and a planet around a Sun-like star (Mayor & Queloz 1995), in just a few decades we have moved from being skeptical about the presence of planets around other stars to the now well-established knowledge that planets are prevalent. Ground-based surveys and the pioneering CoRoT mission gave us the first glimpses of a fact the Kepler mission finally solidified – that there are more planets in our galaxy than there are stars. This started a paradigm shift in the way we think about planetary systems.

TESS and the many more planets around bright stars it will undoubtedly continue to give us, coupled with RVs of unprecedented precision from the most modern spectrographs (e.g. ESPRESSO and EXPRES), will allow us to study less massive planets in wider orbits with improved accuracy. CHEOPS has already lead to the improvement of the radius estimates and ephemerides of several planets, as well as the discovery of additional ones, and will continue to do so in the coming years. In the near future, with its onboard coronagraph,

JWST will have the capability to directly image planets around bright stars, as well as probe exoplanet atmospheres using infrared transit spectroscopy. The discoveries that JWST will lead to will certainly propel us into the next era of exoplanet science.

Unfortunately, questions like "How common is the Solar system architecture?" will continue to remain unanswered for the next few years. However, PLATO, with its large field of view, long observing windows and asteroseismology capabilities, will allow us to know our stars, while perhaps finding the first true Earth analogs, and potentially even Earth 2.0.

5.2 Reflection and Future work

The last pages relate the first steps in my personal journey on the characterisation of exoplanets. The first stages of my PhD involved learning the basics as well as the state-of-the-art of exoplanet detection via transit photometry and Doppler spectroscopy. I have been actively working on improving these skills, and I have thus learned to master these most successful methods which allow us to transform stellar photons into worlds. This culminated in applying these methods to the case of the exoplanets orbiting around TOI-1260. For the time left in my PhD, I plan to use and improve the learned techniques to characterise more exoplanets.

The multi-dimensional Gaussian Process technique that I learned to analyse the data of TOI-1260 is relatively new. As a next step I plan to analyse public data of already published active stars with planets that were analysed with more precarious methods. This will allow me to improve the mass and radius measurements of such planets, and to understand better the underlying activity signals. The results from such a project will be highly valuable for the community given this kind of analysis is scarce. Additional motivation comes from the dearth of precise exoplanet parameters so eagerly needed for characterisation, as I have highlighted in previous chapters.

While analysing the dataset of TOI-1260, one of the most intriguing aspects of the analysis that caught my attention was the fact that the activity indicator I used to measure the planet masses was the S-index. By analysing more active stars in a similar way, I will investigate if S-index is the best indicator

of activity for all active stars, or if it is a case-by-case situation. By doing more modelling of active stars, I plan to learn more about how to remove the activity to recover the most important thing – the planets.

I will also continue to analyse new exoplanet systems unveiled by TESS data. With the expertise I have accumulated, I will be able to perform a faster analysis than for my previous paper. I also add that TOI-1260 was a particularly complicated system, and thus I believe most other systems would be relatively easy to solve in comparison. Alternatively, if a system does turn out to be more complicated, it would be a challenge that I am willing to take and learn more from.

I note, however, that leading new projects which require new data is subject to data availability. While the global pandemic situation is improving, many observatories around the world have been closed. With them, learning opportunities in the form of telescope observations as well as the RV data needed to measure the masses have decreased. The latter may jeopardise my access to new RV datasets – a possibility that makes reanalysing known systems highly attractive.

In summary, I will continue with the characterisation of exoplanets by applying the methods I have learned. At the same time, while analysing different datasets, I will investigate how activity can be modelled to remove stellar induced signals from RVs and detect exoplanets. Step by step, this will contribute to the transformation of photons into worlds.

Bibliography

- Aigrain S., Hodgkin S. T., Irwin M. J., Lewis J. R., Roberts S. J., 2015, MNRAS, 447, 2880
- Alonso R., et al., 2004, ApJL, 613, L153
- Andersen J. M., Korhonen H., 2015, MNRAS, 448, 3053
- Baglin A., et al., 2006, in 36th COSPAR Scientific Assembly. p. 3749
- Bakos G., Noyes R. W., Kovács G., Stanek K. Z., Sasselov D. D., Domsa I., 2004, PASP, 116, 266
- Bakos G. Á., et al., 2013, PASP, 125, 154
- Ballard S., et al., 2011, ApJ, 743, 200
- Barragán O., Gandolfi D., Antoniciello G., 2019a, MNRAS, 482, 1017
- Barragán O., et al., 2019b, MNRAS, 490, 698
- Bedding T. R., et al., 2001, ApJL, 549, L105
- Beichman C., et al., 2014, PASP, 126, 1134
- Benz W., et al., 2021, Experimental Astronomy, 51, 109
- Boccaletti A., 2011, in Beaulieu J. P., Dieters S., Tinetti G., eds, Astronomical Society of the Pacific Conference Series Vol. 450, Molecules in the Atmospheres of Extrasolar Planets. p. 163

- Boisse I., Bouchy F., Hébrard G., Bonfils X., Santos N., Vauclair S., 2011, *A&A*, 528, A4
- Bond I. A., et al., 2004, *ApJL*, 606, L155
- Borucki W. J., 2017, *Proceedings of the American Philosophical Society*, 161, 38
- Borucki W. J., et al., 2010, *Science*, 327, 977
- Borucki W. J., et al., 2011, *ApJ*, 736, 19
- Brewer J. M., et al., 2020, *AJ*, 160, 67
- Cabrera J., Csizmadia S., Erikson A., Rauer H., Kirste S., 2012, *A&A*, 548, A44
- Campbell B., Walker G. A. H., Yang S., 1988, *ApJ*, 331, 902
- Chabrier G., Johansen A., Janson M., Rafikov R., 2014, in Beuther H., Klessen R. S., Dullemond C. P., Henning T., eds, *Protostars and Planets VI*. p. 619, doi:10.2458/azu_uapress_9780816531240-ch027
- Charbonneau D., et al., 2009, *Nature*, 462, 891
- Ciardi D. R., Beichman C. A., Horch E. P., Howell S. B., 2015, *ApJ*, 805, 16
- Collier Cameron A., 2016, *Extrasolar Planetary Transits*. Springer International Publishing, p. 89, doi:10.1007/978-3-319-27458-4_2
- Collier Cameron A., et al., 2020, *arXiv e-prints*, p. arXiv:2011.00018
- Cosentino R., et al., 2012, in *Ground-based and Airborne Instrumentation for Astronomy IV*. p. 84461V, doi:10.1117/12.925738
- Cumming A., Butler R. P., Marcy G. W., Vogt S. S., Wright J. T., Fischer D. A., 2008, *PASP*, 120, 531
- Davis A. B., Cisewski J., Dumusque X., Fischer D. A., Ford E. B., 2017, *ApJ*, 846, 59
- Díaz R. F., Almenara J. M., Santerne A., Moutou C., Lethuillier A., Deleuil M., 2014, *MNRAS*, 441, 983

- Dumusque X., 2018, *A&A*, 620, A47
- Dumusque X., Udry S., Lovis C., Santos N. C., Monteiro M. J. P. F. G., 2011, *A&A*, 525, A140
- Fischer D. A., Valenti J., 2005, *ApJ*, 622, 1102
- Fulton B. J., et al., 2017, *AJ*, 154, 109
- Gaudi B. S., et al., 2020a, arXiv e-prints, p. arXiv:2001.06683
- Gaudi B. S., Christiansen J. L., Meyer M. R., 2020b, arXiv e-prints, p. arXiv:2011.04703
- Gautier Thomas N. I., et al., 2012, *ApJ*, 749, 15
- Georgieva I. Y., et al., 2021, arXiv e-prints, p. arXiv:2104.05653
- Giacalone S., et al., 2021, *AJ*, 161, 24
- Gillon M., Jehin E., Magain P., Chantry V., Hutsemékers D., Manfroid J., Queloz D., Udry S., 2011, in *European Physical Journal Web of Conferences*. p. 06002 (arXiv:1101.5807), doi:10.1051/epjconf/20101106002
- Ginzburg S., Schlichting H. E., Sari R., 2016, *ApJ*, 825, 29
- Ginzburg S., Schlichting H. E., Sari R., 2018, *MNRAS*, 476, 759
- Grziwa S., Pätzold M., Carone L., 2012, *MNRAS*, 420, 1045
- Gupta A., Schlichting H. E., 2019, *MNRAS*, 487, 24
- Gupta A., Schlichting H. E., 2020, *MNRAS*, 493, 792
- Hastings W. K., 1970, *Biometrika*, 57, 97
- Hatzes A. P., 2016, *The Radial Velocity Method for the Detection of Exoplanets*. Springer International Publishing, p. 3, doi:10.1007/978-3-319-27458-4_1
- Hatzes A. P., Cochran W. D., 1993, *ApJ*, 413, 339
- Hatzes A. P., Rauer H., 2015, *ApJL*, 810, L25

- Haywood R. D., et al., 2014, MNRAS, 443, 2517
- Hippke M., Heller R., 2019, A&A, 623, A39
- Howard A. W., et al., 2010, Science, 330, 653
- Howell S. B., et al., 2014, PASP, 126, 398
- Irwin J. M., Berta-Thompson Z. K., Charbonneau D., Dittmann J., Falco E. E., Newton E. R., Nutzman P., 2015, in 18th Cambridge Workshop on Cool Stars, Stellar Systems, and the Sun. pp 767–772 ([arXiv:1409.0891](#))
- Jenkins J. M., et al., 2010, ApJL, 713, L87
- Jenkins J. M., et al., 2016, in Chiozzi G., Guzman J. C., eds, Society of Photo-Optical Instrumentation Engineers (SPIE) Conference Series Vol. 9913, Software and Cyberinfrastructure for Astronomy IV. p. 99133E, doi:10.1117/12.2233418
- Jurgenson C., Fischer D., McCracken T., Sawyer D., Szymkowiak A., Davis A., Muller G., Santoro F., 2016, in Evans C. J., Simard L., Takami H., eds, Society of Photo-Optical Instrumentation Engineers (SPIE) Conference Series Vol. 9908, Ground-based and Airborne Instrumentation for Astronomy VI. p. 99086T ([arXiv:1606.04413](#)), doi:10.1117/12.2233002
- Kovács G., Zucker S., Mazeh T., 2002, A&A, 391, 369
- Latham D. W., Mazeh T., Stefanik R. P., Mayor M., Burki G., 1989, Nature, 339, 38
- Lopez E. D., Fortney J. J., 2014, ApJ, 792, 1
- Mandel K., Agol E., 2002, ApJL, 580, L171
- Mayo A. W., et al., 2018, AJ, 155, 136
- Mayor M., Queloz D., 1995, Nature, 378, 355
- Mayor M., et al., 2003, The Messenger, 114, 20
- Mazeh T., Holczer T., Faigler S., 2016, A&A, 589, A75
- Metropolis N., Rosenbluth A. W., Rosenbluth M. N., Teller A. H., Teller E., 1953, Journal of Computational Physics, 21, 1087

- Meunier N., Desort M., Lagrange A. M., 2010, *A&A*, 512, A39
- Morton T. D., 2012, *ApJ*, 761, 6
- Nutzman P., Charbonneau D., 2008, *PASP*, 120, 317
- Owen J. E., Wu Y., 2013, *ApJ*, 775, 105
- Parviainen H., et al., 2019, *A&A*, 630, A89
- Pecaut M. J., Mamajek E. E., 2013, *APJS*, 208, 9
- Pepe F. A., et al., 2010, in McLean I. S., Ramsay S. K., Takami H., eds, *Society of Photo-Optical Instrumentation Engineers (SPIE) Conference Series Vol. 7735, Ground-based and Airborne Instrumentation for Astronomy III*. p. 77350F, doi:10.1117/12.857122
- Pepe F., et al., 2020, arXiv e-prints, p. arXiv:2010.00316
- Pepper J., et al., 2007, *PASP*, 119, 923
- Perryman M., 2018, *Transits*, 2 edn. Cambridge University Press, p. 153–328, doi:10.1017/9781108304160.007
- Persson C. M., et al., 2019, *A&A*, 628, A64
- Petigura E. A., Marcy G. W., Howard A. W., 2013, *ApJ*, 770, 69
- Petigura E. A., et al., 2018, *AJ*, 155, 89
- Pollacco D. L., et al., 2006, *PASP*, 118, 1407
- Pont F., Knutson H., Gilliland R. L., Moutou C., Charbonneau D., 2008, *MNRAS*, 385, 109
- Prša A., et al., 2016, *AJ*, 152, 41
- Quanz S., 2019, in *EPSC-DPS Joint Meeting 2019*. pp EPSC–DPS2019–327
- Queloz D., et al., 2009, *A&A*, 506, 303
- Rajpaul V., Aigrain S., Osborne M. A., Reece S., Roberts S., 2015, *MNRAS*, 452, 2269

- Rajpaul V., Aigrain S., Roberts S., 2016, MNRAS, 456, L6
- Rauer H., et al., 2014, Experimental Astronomy, 38, 249
- Reiners A., Bean J. L., Huber K. F., Dreizler S., Seifahrt A., Czesla S., 2010, ApJ, 710, 432
- Renner S., Rauer H., Erikson A., Hedelt P., Kabath P., Titz R., Voss H., 2008, A&A, 492, 617
- Ricker G. R., et al., 2015, Journal of Astronomical Telescopes, Instruments, and Systems, 1, 014003
- Rodríguez Martínez R., Stevens D. J., Gaudi B. S., Schulze J. G., Panero W. R., Johnson J. A., Wang J., 2021, ApJ, 911, 84
- Rogers J. G., Gupta A., Owen J. E., Schlichting H. E., 2021, arXiv e-prints, p. arXiv:2105.03443
- Sanchis-Ojeda R., Winn J. N., Fabrycky D. C., 2013, Astronomische Nachrichten, 334, 180
- Savitzky A., Golay M. J. E., 1964, Analytical Chemistry, 36, 1627
- Seager S., Mallén-Ornelas G., 2003, ApJ, 585, 1038
- Smith J. C., et al., 2012, PASP, 124, 1000
- Smith A. M. S., et al., 2017, MNRAS, 464, 2708
- Soter S., 2006, AJ, 132, 2513
- Southworth J., Wheatley P. J., Sams G., 2007, MNRAS, 379, L11
- Spergel D., et al., 2015, arXiv e-prints, p. arXiv:1503.03757
- Stevens D. J., Gaudi B. S., 2013, PASP, 125, 933
- Struve O., 1952, The Observatory, 72, 199
- Stumpe M. C., et al., 2012, PASP, 124, 985
- Suárez Mascareño A., et al., 2020, A&A, 639, A77

- Sumi T., et al., 2010, *ApJ*, 710, 1641
- Tal-Or L., et al., 2013, *A&A*, 553, A30
- The LUVOIR Team 2019, arXiv e-prints, p. arXiv:1912.06219
- Tinetti G., et al., 2021, arXiv e-prints, p. arXiv:2104.04824
- Turbet M., Bolmont E., Ehrenreich D., Gratier P., Leconte J., Selsis F., Hara N., Lovis C., 2020, *A&A*, 638, A41
- Van Eylen V., Agentoft C., Lundkvist M. S., Kjeldsen H., Owen J. E., Fulton B. J., Petigura E., Snellen I., 2018, *MNRAS*, 479, 4786
- Van Eylen V., et al., 2021, arXiv e-prints, p. arXiv:2101.01593
- Vanderburg A., Johnson J. A., 2014, *PASP*, 126, 948
- Weiss L. M., et al., 2018, *AJ*, 155, 48
- Winn J. N., 2010, *Exoplanet Transits and Occultations*. University of Arizona Press, Tucson, AZ, pp 55–77
- Wolszczan A., Frail D. A., 1992, *Nature*, 355, 145
- de Beurs Z. L., et al., 2020, arXiv e-prints, p. arXiv:2011.00003

